

Inter-Turn Short Circuit Fault and High Resistance Connection in Stator of Doubly-Fed Induction Generators

M. Afshari¹, M. Moosavi^{1*}, M. B. Abadi² and Sérgio M. A. Cruz²

1. Department of Electrical Engineering, Hamedan University of Technology, Hamedan, Iran.

2. Department of Electrical and Computer Engineering, University of Coimbra, Coimbra, Portugal.

Received Date 30 July 2021; Revised Date 05 August 2021; Accepted Date 23 August 2021

*Corresponding author: moosavi@hut.ac.ir (Seyed-Mohammad M. Moosavi)

Abstract

Doubly-fed induction generators (DFIGs) have been widely used in wind turbines (WTs) installed in the last decades. These generators are prone to some faults that could deteriorate their performance and even lead to their outage from the network. Stator inter-turn short-circuits (SITSCs) and high resistance connections (HRCs) in the stator are two major types of faults that cause electrical asymmetry in the stator circuit. Yet, SITSCs are more noticeable, and require an immediate scrutiny. Hence, if an HRC can be distinguished from a SITSC fault, the immediate outage of WT can be avoided in the case of an HRC. In this paper, both types of faults are studied and compared, being their detection performed using appropriate fault indices obtained from the stator current, rotor current, and rotor modulating voltage signals, all available in the control system of DFIG. Several fault severity indices are proposed for a better evaluation of the fault extension, and the discrimination between SITSC and HRC is discussed. The performance of the defined fault indices is verified using a magnetic equivalent circuit model of DFIG and an experimental setup with the DFIG running at several operating conditions.

Keywords: *Fault detection; Doubly-fed induction generators; Stator inter-turn short circuits; High resistance connections.*

1. Introduction

Renewable energy systems have been developed sharply in the last decade, and the wind energy is the pioneer of installed power capacity in the world. Doubly-Fed Induction Generators (DFIGs) based on wind turbines (WTs) are the most utilized technology due to their advantages. DFIGs have the capability of active and reactive power control, and employ an induction machine and partial power converter, and thus lead to a lower cost compared to the other technologies [1, 2].

WTs are usually located in more adverse conditions in comparison to the steam and hydro turbines. Furthermore, it is not easy to access a generator located more than one hundred meters above the ground. A high failure rate of WT unfavorably affects the beneficial gain of the wind energy conversion systems. Thus appropriate condition monitoring methods and detection of faults at an early stage lead to lower costs in terms of operation and maintenance (O&M) [3-5]. As a main component of a WT, the generator is vulnerable to different electrical and

mechanical faults [6, 7]. About 30-40% of generator faults are linked to the stator [4], which primarily arise in the form of stator inter-turn short circuits (SITSCs) [8]. If a SITSC fault is not detected at an early stage, it may lead to a severe damage to the generator. Another stator-related fault is the high resistance connection (HRC) in the stator circuit. HRC is a common problem in the connections of industrial machines, which mainly occurs due to loosening of connections or pitting, corrosion or contamination of contact surfaces. The aggressive environments of DFIGs make these generators prone to the HRC fault. Due to the additional losses in HRC, the local heating may cause an open circuit or a short-circuit failure in the system [9, 10]. Although the nature of SITSC and HRC faults is different, both introduce an asymmetry in the stator circuit and flux distribution of the machine. The usual methods for detecting SITSC and HRC are based on asymmetry variation in the three-phase system, and some indicators such as zero-sequence voltage and negative-sequence current have been

proposed [9, 11]. Nevertheless, SITSC and HRC require different actions. SITSC develops very quickly, and requires fast remedial actions, while HRC is a gradual event that usually requires no immediate action. Therefore, it is essential to distinguish these two origins of asymmetry.

SITSC and HRC in the stator of DFIG have been investigated primarily individually. In [12], the stator current combined with the extended Park's vector and wavelet transform has been utilized for the detection of SITSC. As the SITSC fault has been modelled by paralleling an external variable resistor with a stator phase circuit, the real nature of the SITSC fault has not been considered. Some SITSC fault indices based on the analysis of the rotor current and search coil voltage have been proposed in [13]. Although an in-depth study on the origin of frequency components in the rotor current has been carried out, only the stand-alone operation of DFIG has been regarded. Also the detection method based on the search coil is an invasive and costly method. The effects of a SITSC fault on the airgap magnetic field spectrum has been studied [14]. The machine has been modelled by the finite element method (FEM), and no control system has been included. A hybrid abc/dq model has been suggested in [15], which models DFIG subjected to a SITSC fault. The wavelet analysis of the stator current signal and its energy has been used for the calculation of the fault index. This study lacks experimental verification, and involves no control system. In [16], by applying short voltage pulses to the rotor terminals, the transient leakage inductances have been evaluated. Then based on a special signal processing technique, the SITSC fault has been figured out. The effects of SITSC faults with different severities and different slot locations on the negative sequence and phase difference of the stator currents have been presented in [17]. The machine has been modelled by FEM, and no control system has been included. Recently, it has been suggested that symmetrical components, Park's vector trajectory, phase difference, and total harmonic distortion of the stator currents could be the indicators of SITSC faults in DFIG [8].

Although the HRC problem has been widely researched in the rotor circuit of DFIG [18-22], this issue on the stator circuit has been far less considered. The electric anomaly of DFIG on both the stator and rotor sides has been studied in [23]. A frequency component in the rotor modulating signal, available in the control system of the DFIG, has been proposed as a fault index. Its superiority in relation to the stator and rotor

current components has been verified. Following that, the work has been extended [10], and based on the wavelet transform, a time-frequency fault indicator has been introduced.

A simulation study has been carried out in order to differentiate SITSC and stator HRC [24]. A normalized energy signal obtained from the wavelet transform of the rotor modulating voltage has been proposed as a diagnostic index. A recent investigation on in-service WTs has shown that the current signature analysis is adequate for fault diagnosis [4]. This approach is more cost-effective and simpler than the time-frequency methods (such as the wavelet transform), making it an acceptable choice.

In this paper, similarly to [25], the induction machine is modelled using a magnetic equivalent circuit (MEC). Then HRC and SITSC are implemented in the stator side. The rotor side converter (RSC), which feeds the rotor of the DFIG, is governed by a vector control system, and the faulty DFIG is operated at sub-synchronous and super-synchronous speeds. The effects of the faults on different signals available are explored, and an approach is proposed for the discrimination between the two types of faults. As a consequence, HRC can be easily distinguished from a SITSC fault, thus avoiding the immediate outage of WT in the case of HRC.

This paper is organized as what follows. First, the DFIG model and its respective control system is presented in Section 2. In Section 3, the operation of DFIG, in the presence of SITSC and HRC faults, is evaluated in the time domain by simulation and experiments. Section 4 deals with the effects of each fault on the specific spectral components of some quantities at different fault severities and operating states of the DFIG including different power injection and speeds, including sub-synchronous and super-synchronous modes of operation. In Section 5, some fault severity indices are proposed for the evaluation of fault extension, and the discrimination method between SITSC and HRC is discussed. Finally, Section 6 draws the main conclusions of this work.

2. Machine Model and DFIG Control System

The modelling of DFIG was performed using the magnetic equivalent circuit (MEC) model of the wound rotor induction machine presented in [19]. HRC in the stator side was modelled by the insertion of an additional resistance in one of the stator phases. For the introduction of SITSC, the model was modified, and the MMF transform matrix (that connects MMF with phase currents)

of the stator was rearranged in order to include the fault by considering the slots that contain the shorted turns while the rotor is healthy. Thus an additional circuit loop containing the shorted turns was added to the stator side. The voltage equation of this additional loop is governed by:

$$0 = R_f i_f + \frac{d\lambda_f}{dt} \quad (1)$$

Where i_f is the short-circuit current, R_f is the sum of the fault resistance and resistance of the shorted turns, and λ_f is the flux linkage associated with the short-circuited turns.

The specifications of WRIM are presented in table 1.

Table 1. Specifications of WRIM

Description	Value	Description	Value
Rated power	4 kW	Rated frequency	50 Hz
Rated stator voltage	254 V	Rated rotor voltage	147 V
Rated stator current	9.4 A	Rated rotor current	11.5 A
Rated speed	1420 rpm	Number of poles	4
Inertia	0.15 kg.m ²	Friction coefficient	N.m.s/rad
Inductances	L _{ls} = 7.9 mH, L _{lr} = 2.9 mH, L _{ms} = 121 mH		
Stator resistance	1.26 Ω	Rotor resistance	0.5 Ω

The rotor of DFIG is fed by RSC, and its stator is directly connected to the grid. Here, a stator-flux-oriented vector control scheme is utilized in order to provide the independent control of the active and reactive powers. The control system of RSC involves two outer and two inner control loops. The reference values of the rotor currents are determined by the desired values of the stator active and reactive powers. Then the current control loops specify the rotor voltages to be applied by RSC based on these reference currents. According to the control of RSC, the stator active and reactive powers are determined by the rotor current components [20]:

$$P_s \cong -\frac{3}{2} \hat{V}_s \frac{L_{ms}}{L_s} i_{qr} \quad (2)$$

$$Q_s \cong \frac{3}{2} \frac{\hat{V}_s^2}{\omega_s L_s} - \frac{3}{2} \hat{V}_s \frac{L_{ms}}{L_s} i_{dr} \quad (3)$$

where L_{ms} is the mutual inductance between the stator and rotor windings, L_s is the stator self-inductance, and \hat{V}_s is the peak value of the stator phase voltage.

Figure 1 shows the control diagram of RSC, the actual DFIG used in the laboratory coupled to an

induction motor drive that acts as a prime mover, and the whole experimental setup. DFIG has some taps along the stator windings in order to facilitate the implementation of SITSC, while the HRC test is accomplished by adding a proper resistance in series with one phase of the stator phases. A variable-speed induction motor drive is mechanically coupled to DFIG in order to impose the required speeds. The DFIG control system was implemented in a dSPACE 1103 platform, which also enabled data measurements.

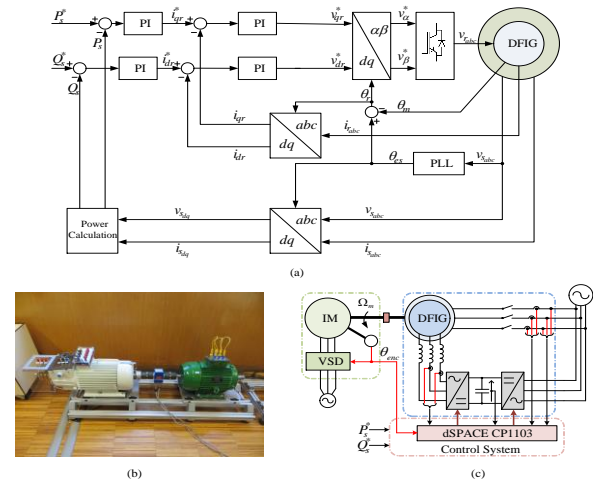


Figure 1. Description of DFIG system: (a) implemented DFIG control system, (b) DFIG (left) coupled to an IM (right), (c) connections diagram of the experimental setup.

3. Electrical Asymmetry in DFIG Stator

In this section, SITSC and HRC in the stator circuit are investigated by simulation and by the experimental tests.

3.1. SITSC

SITSC was implemented with different severities. The waveforms of the stator currents and rotor currents when 7 turns are shorted in the stator winding are illustrated in figures 2 and 3. Also different operating conditions (active power and speed) including sub-synchronous and super-synchronous operation of DFIG were considered while the fault was present. The current rms values of the faulty phase in the stator and also in one phase of the rotor for these operating points are documented in tables 2 and 3. As expected, due to the presence of the current controllers, the current values in the faulty case do not deviate much from the healthy ones.

3.2. HRC

Similar to the previous sub-section, the waveforms of the stator and rotor currents are shown in figures 4 and 5. Here, an additional resistance with 150% of the stator resistance value

was inserted in series with one stator phase. As before, different operating conditions (active power and speed) including sub-synchronous and super-synchronous operations of DFIG were

considered. The rms values of current in the stator faulty phase and in one rotor phase are presented in tables 4 and 5.

Table 2. Simulation: rms values of stator and rotor currents with 7 short-circuited stator turns.

Power injected into the grid	$P_s = -2 \text{ kW } Q_s = 0 \text{ VAR}$				$P_s = -1 \text{ kW } Q_s = 0 \text{ VAR}$			
	1350		1650		1350		1650	
Shaft speed (rpm)	Healthy	Faulty	Healthy	Faulty	Healthy	Faulty	Healthy	Faulty
I_s (A)	4.546	4.474	4.541	4.463	2.300	2.198	2.284	2.177
I_r (A)	8.799	8.950	8.795	8.952	5.615	5.809	5.597	5.782

Table 3. Measured rms values of stator and rotor currents with 7 short-circuited stator turns.

Power injected into the grid	$P_s = -2 \text{ kW } Q_s = 0 \text{ VAR}$				$P_s = -1 \text{ kW } Q_s = 0 \text{ VAR}$			
	1350		1650		1350		1650	
Shaft speed (rpm)	Healthy	Faulty	Healthy	Faulty	Healthy	Faulty	Healthy	Faulty
I_s (A)	4.367	4.258	4.348	4.235	2.187	2.067	2.170	2.074
I_r (A)	8.711	8.939	8.580	8.802	5.556	5.739	5.434	5.632

Table 4. Simulation; rms values of stator and rotor currents with HRC 1.5R_s.

Power injected into the grid	$P_s = -2 \text{ kW } Q_s = 0 \text{ VAR}$				$P_s = -1 \text{ kW } Q_s = 0 \text{ VAR}$			
	1350		1650		1350		1650	
Shaft speed (rpm)	Healthy	Faulty	Healthy	Faulty	Healthy	Faulty	Healthy	Faulty
I_s (A)	4.546	4.521	4.541	4.513	2.300	2.288	2.284	2.270
I_r (A)	8.799	8.832	8.795	8.828	5.615	5.643	5.597	5.643

Table 5. Measured rms values of stator and rotor currents with HRC = 1.5R_s.

Power injected into the grid	$P_s = -2 \text{ kW } Q_s = 0 \text{ VAR}$				$P_s = -1 \text{ kW } Q_s = 0 \text{ VAR}$			
	1350		1650		1350		1650	
Shaft speed (rpm)	Healthy	Faulty	Healthy	Faulty	Healthy	Faulty	Healthy	Faulty
I_s (A)	4.367	4.456	4.348	4.442	2.187	2.207	2.170	2.181
I_r (A)	8.711	8.788	8.580	8.698	5.556	5.540	5.434	5.454

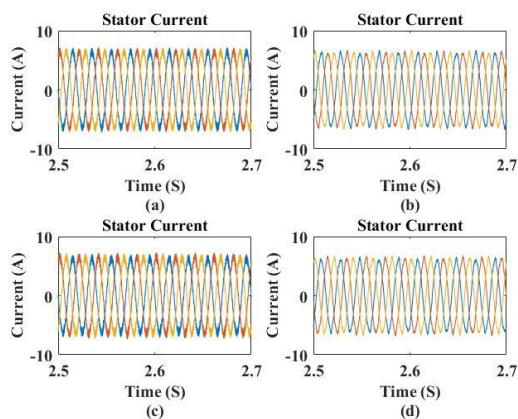


Figure 2. Stator phase currents a) healthy–simulation, b) healthy–experiment, c) 7 short-circuited turns–simulation, d) 7 short-circuited turns–experiment.

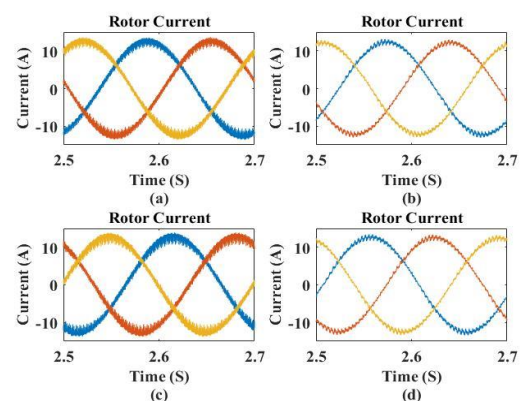


Figure 3. Rotor phase currents a) healthy–simulation, b) healthy–experiment, c) 7 short-circuited turns–simulation, d) 7 short-circuited turns–experiment.

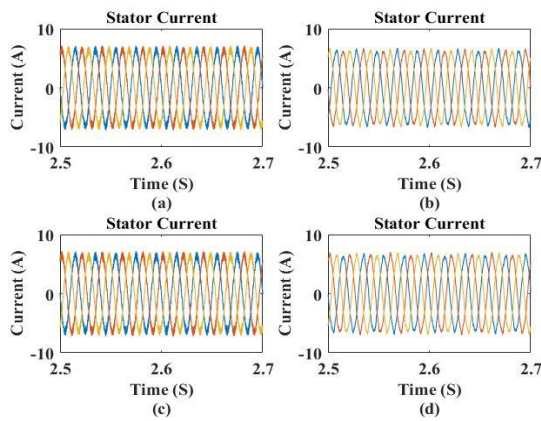


Figure 4. Stator phase currents a) healthy–simulation, b) healthy–experiment, c) HRC = 1.5R_s–simulation, d) HRC = 1.5R_s–experiment.

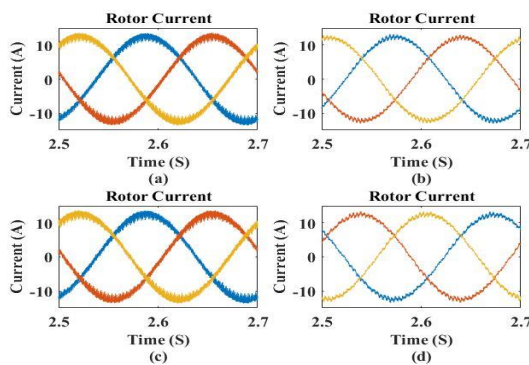


Figure 5. Rotor phase currents a) healthy – simulation, b) healthy–experiment, c) HRC = 1.5R_s–simulation, d) HRC = 1.5R_s–experiment.

4. Frequency Tracking in an Electrically Asymmetric Stator

Different approaches have been proposed for fault detection in electrical machines. In signal-based methods, fault signatures of some machine quantities have been monitored with proper signal processing methods [28]. Thus it is necessary to appropriately determine the fault signatures in specific signals, and then track them to be aware of any abnormal behaviour. The major frequency components introduced for detection of asymmetry in the stator circuit of DFIG are as follow [23]:

$-f_s$ (inverse-sequence component) in the stator current spectrum; this index could be obtained by applying FFT to the space vector of stator current.
 $(2-s)f_s$ in rotor current spectrum, which arises

from reverse rotating magnetic field due to the stator asymmetry.

$(2-s)f_s$ in the rotor modulating voltage signal spectrum, which is excited by the control system to attenuate the fault components in the rotor currents.

At this stage, the frequency components of the suggested quantities were obtained with DFIG in the healthy and faulty conditions including SITSC and HRC.

4.1. SITSC

The stator current frequency spectra of the healthy and faulty DFIG (1, 4, and 7 short-circuited stator turns) operating at sub-synchronous speed with active power injection obtained by simulation are compared in figure 6. The increase in the amplitude of the $-f_s$ component is notable when the fault severity elevates. In figure 7, the experimental results are presented, which show a good agreement with the simulation results.

Tables 6-8 summarize the results obtained for SITSC fault indices when DFIG operates at sub-synchronous and super-synchronous speeds, while injecting different values of active power into the grid. It was recognized that all regarded indices were sensitive to the SITSC faults. The rotor modulating signal index shows a better performance with a larger increase in magnitude and also more pronounced magnitude for each faulty condition.

4.2. HRC

Figure 8 shows the harmonic spectra of DFIG stator current in healthy and faulty conditions (1.5R_s HRC), operating at sub-synchronous speed with active power injection obtained by simulation and experiments. Tables 9-11 present the results obtained for the HRC fault frequency components when DFIG operates at sub-synchronous and super-synchronous speeds while injecting different values of active power into the grid. It is possible to verify that all the regarded components increase in amplitude with the HRC severity. Again, the rotor modulating voltage signal fault component shows a better performance with a higher increase in magnitude and a more measurable magnitude for each faulty condition.

Table 6. Stator current SITSC fault frequency component for the operation of DFIG in healthy and faulty conditions at sub-synchronous and super-synchronous speeds (in dB).

Power injection to grid	P _s = -2 kW Q _s = 0 Var		P _s = -1 kW Q _s = 0 Var	
Shaft speed	1350 rpm	1650 rpm	1350 rpm	1650 rpm
Healthy	-66.42	-66.28	-61.00	-58.40
1-turn shorted	-58.99	-59.25	-52.23	-54.10
4-turns shorted	-45.58	-45.26	-35.48	-35.43
7-turns shorted	-33.93	-33.83	-25.93	-25.85

Table 7. Rotor current SITSC fault frequency component for the operation of DFIG in healthy and faulty conditions at sub-synchronous and super-synchronous speeds (in dB).

Power injection to grid	$P_s = -2 \text{ kW } Q_s = 0 \text{ Var}$		$P_s = -1 \text{ kW } Q_s = 0 \text{ Var}$	
	1350 rpm	1650 rpm	1350 rpm	1650 rpm
Shaft speed	1350 rpm	1650 rpm	1350 rpm	1650 rpm
Healthy	-83.76	-84.84	-70.29	-74.85
1-turn shorted	-62.87	-63.63	-60.41	-58.80
4-turns shorted	-52.74	-51.44	-48.69	-47.99
7-turns shorted	-48.31	-47.54	-44.38	-44.16

Table 8. Rotor modulating signal SITSC fault frequency component for the operation of DFIG in healthy and faulty conditions at sub-synchronous and super-synchronous speeds (in dB).

Power injection to grid	$P_s = -2 \text{ kW } Q_s = 0 \text{ Var}$		$P_s = -1 \text{ kW } Q_s = 0 \text{ Var}$	
	1350 rpm	1650 rpm	1350 rpm	1650 rpm
Shaft speed	1350 rpm	1650 rpm	1350 rpm	1650 rpm
Healthy	-53.11	-51.38	-44.23	-45.91
1-turn shorted	-32.62	-32.47	-34.32	-31.13
4-turns shorted	-22.68	-19.66	-22.75	-19.77
7-turns shorted	-18.84	-15.65	-18.72	-15.66

Table 9. Stator current HRC fault frequency component for the operation of DFIG in healthy and faulty conditions at sub-synchronous and super-synchronous speeds (in dB).

Power injection to grid		$P_s = -2 \text{ kW } Q_s = 0 \text{ Var}$		$P_s = -1 \text{ kW } Q_s = 0 \text{ Var}$	
		1350 rpm	1650 rpm	1350 rpm	1650 rpm
Healthy	Simulation	-66.42	-66.28	-61.00	-58.40
	Experiment	-49.55	-49.25	-45.81	-45.29
Faulty ($R_s * 0.6$)	Simulation	-58.27	-57.93	-54.47	-54.15
	Experiment	-45.23	-44.89	-43.10	-42.79
Faulty ($R_s * 1.5$)	Simulation	-41.97	-41.54	-41.32	-41.06
	Experiment	-37.30	-36.09	-37.74	-34.91

Table 10. Rotor current HRC fault frequency component for the operation of DFIG in healthy and faulty conditions at sub-synchronous and super-synchronous speeds (in dB).

Power injection to grid		$P_s = -2 \text{ kW } Q_s = 0 \text{ Var}$		$P_s = -1 \text{ kW } Q_s = 0 \text{ Var}$	
		1350 rpm	1650 rpm	1350 rpm	1650 rpm
Healthy	Simulation	-83.76	-84.84	-70.29	-74.85
	Experiment	-53.99	-55.50	-59.39	-56.66
Faulty ($R_s * 0.6$)	Simulation	-70.81	-70.34	-62.41	-62.11
	Experiment	-48.45	-47.92	-52.77	-51.98
Faulty ($R_s * 1.5$)	Simulation	-44.79	-43.90	-46.50	-45.80
	Experiment	-37.24	-36.23	-39.43	-36.89

Table 11. Rotor modulating signal HRC fault frequency component for the operation of DFIG in healthy and faulty conditions at sub-synchronous and super-synchronous speeds (in dB).

Power injection to grid		$P_s = -2 \text{ kW } Q_s = 0 \text{ Var}$		$P_s = -1 \text{ kW } Q_s = 0 \text{ Var}$	
		1350 rpm	1650 rpm	1350 rpm	1650 rpm
Healthy	Simulation	-53.11	-51.38	-44.23	-45.91
	Experiment	-31.20	-24.52	-39.09	-31.33
Faulty ($R_s * 0.6$)	Simulation	-40.27	-39.14	-36.22	-35.31
	Experiment	-25.81	-18.09	-32.47	-24.79
Faulty ($R_s * 1.5$)	Simulation	-14.68	-12.52	-20.61	-17.66
	Experiment	-15.14	-15.25	-19.77	-11.81

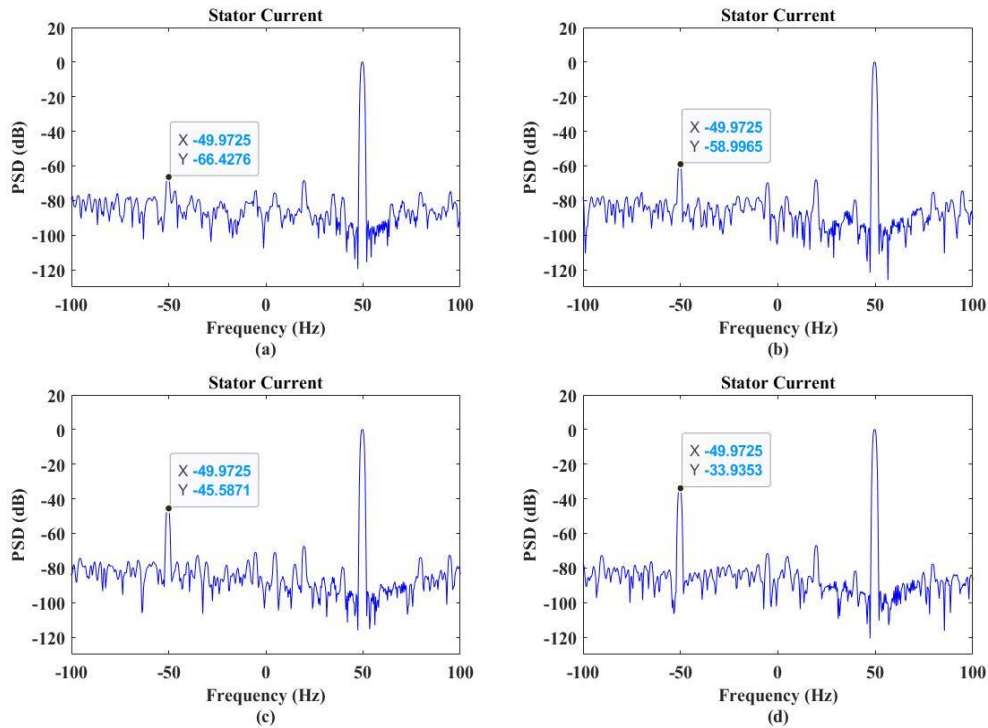


Figure 6. Simulation results showing a comparison of the spectra of the stator current for DFIG in healthy and SITSC cases ($n_m = 1350$ rpm, $P_s = -2$ kW, $Q_s = 0$ kVAr) a) healthy, b) 1-turn shorted, c) 4-turns shorted, d) 7-turns shorted.

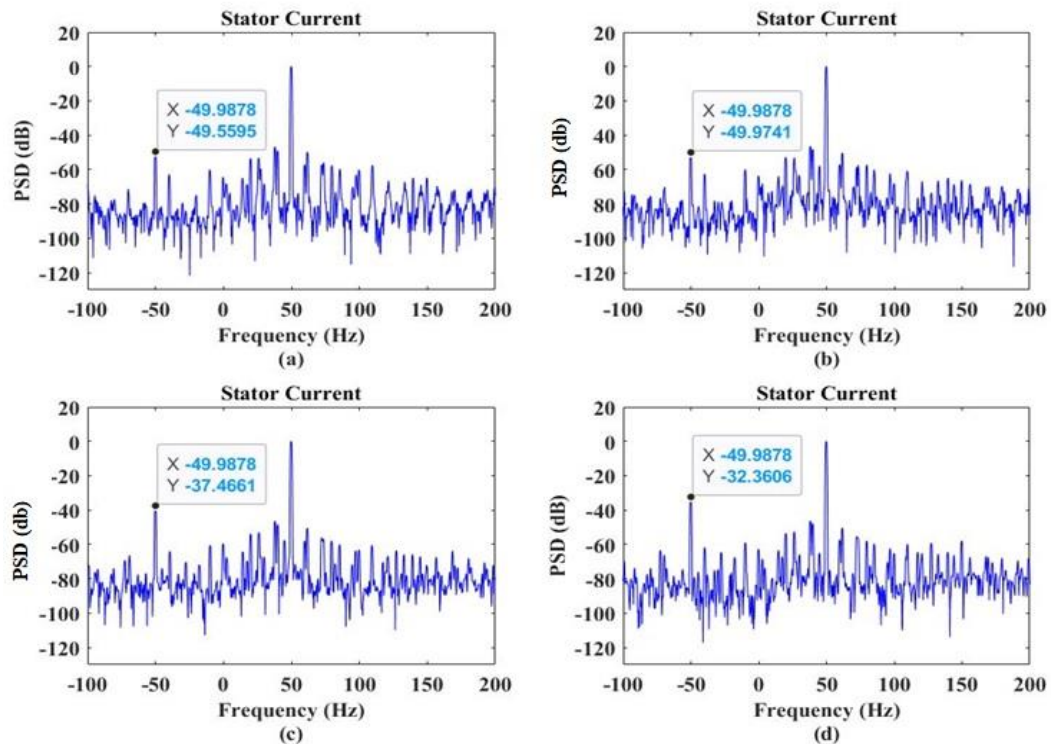


Figure 7. Experimental results showing a comparison of the spectra of the stator current for DFIG in healthy and SITSC cases ($n_m = 1350$ rpm, $P_s = -2$ kW, $Q_s = 0$ kVAr) a) healthy, b) 1-turn shorted, c) 4-turns shorted, d) 7-turns shorted.

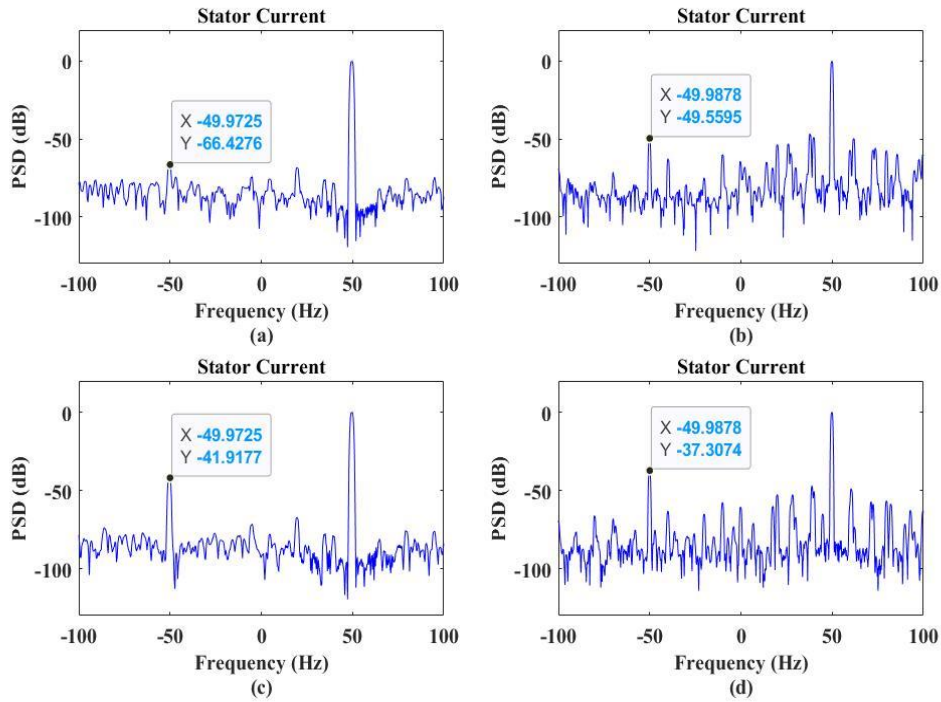


Figure 8. Stator current spectra of DFIG in healthy and HRC ($n_m = 1350$ rpm, $P_s = -2$ kW, $Q_s = 0$ kVAr) a) healthy–simulation, b) healthy–experiment, c) HRC 1.5R_s–simulation, d) HRC 1.5R_s–experiment.

5. Discussion

The results obtained clearly show that independence of the sub-synchronous or super-synchronous operation of DFIG or amount of injected power to the grid, all the regarded components are sensitive to the stator electric asymmetry originated from SITSC or HRC. For a more accurate comparison between the studied frequency components, some fault sensitivity indices were defined as follow:

$$FS_{i_s} = 100 \times \frac{FI_{i_s, fault}}{FI_{i_s, healthy}} \quad (4)$$

$$FS_{i_r} = 100 \times \frac{FI_{i_r, fault}}{FI_{i_r, healthy}} \quad (5)$$

$$FS_{v_r} = 100 \times \frac{FI_{v_r, fault}}{FI_{v_r, healthy}} \quad (6)$$

Where FS is the fault severity factor and FI is the fault index component.

For a deeper analysis, the sensitivity of these severity factors was evaluated for both SITSC and HRC at different fault severities. Figure 9 shows the variation in the fault severity factors due to different SITSC fault intensities. These results were obtained with DFIG operating at 1350 rpm while injecting 2 kW into the grid. Figure 10

demonstrates the variations in FS for a HRC fault. It is apparent that the rotor modulating voltage signal is more sensitive to both the SITSC and HRC faults, and thus is the best choice for condition monitoring of the stator circuit of DFIG. According to these figures, a 7 shorted turns fault approximately leads to the same FS (based on the rotor modulating voltage signal) as a 100%R_s HRC fault. As each phase of the stator winding contains 6 coils with 30 turns each, 7 shorted turns correspond to nearly 4% of the total number of stator turns shorted.

In the case of HRC, the current controllers decrease the current asymmetric condition by applying unbalanced rotor voltage modulating signals. Hence, the rotor modulating signal index is increased while the stator and rotor currents are not significantly affected. However, when a SITSC occurs, the controllers do not have similar capabilities. The SITSC fault creates an opposing flux, which causes an internal asymmetry in the magnetic flux distribution. The DFIG controllers apply unbalanced rotor voltages to reduce the asymmetry, though the situation will not be exactly as in the HRC case, and the machine currents, especially the stator currents, are still unbalanced, to some extent. In other words, for a specific value of the rotor modulating signal fault index, the stator current fault index has a greater magnitude in the case of SITSC. Consequently, the simultaneous tracking of the rotor modulating

signal and the stator current fault frequency components could help to discriminate between the two faults.

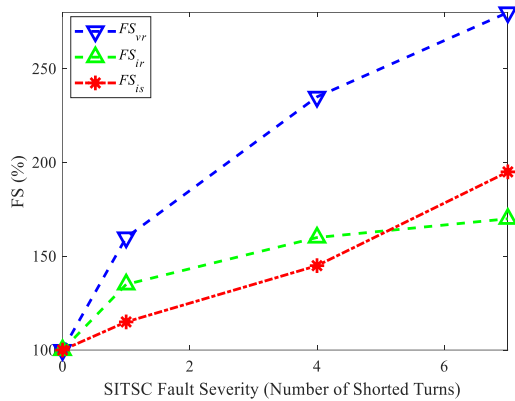


Figure 9. Fault sensitivity due to different SITSC severities at 1350 rpm, $P_s = -2$ kW, $Q_s = 0$ Var.

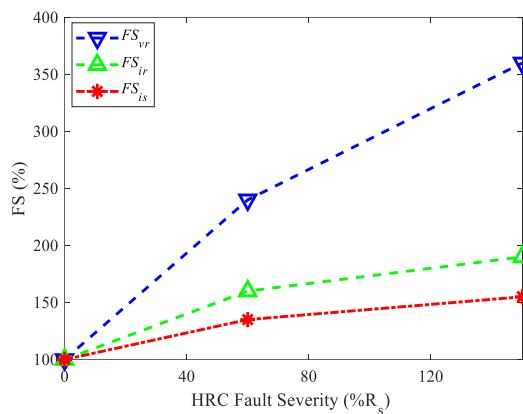


Figure 10. Fault sensitivity due to different HRC severities at 1350 rpm, $P_s = -2$ kW, $Q_s = 0$ Var.

6. Conclusions

In this paper, SITSC and HRC in the stator circuit were investigated as the two main origins of stator electrical asymmetry in doubly-fed induction generators. The capability of the stator current, rotor current, and rotor modulating voltage spectra for the detection and isolation of the two types of faults were analyzed. The simulation and experimental results demonstrated that the combined monitoring of the rotor voltage modulating signal and the stator current fault frequencies could be employed in order to detect and discriminate the SITSC and HRC faults. In this way, an appropriate course of action could be selected, leading to reduced financial losses.

7. Acknowledgment

This journal paper is the extended version of conference paper that was presented at the 2021 7th Iran Wind Energy conference (IWEC 2021).

8. References

- [1] T. Ackermann, *Wind Power in Power Systems*, 2nd Ed. John Wiley and Sons, 2012.
- [2] J. Faiz and S.M.M. Moosavi, "Eccentricity fault detection—From induction machines to DFIG—A review," *Renewable and Sustainable Energy Reviews*, Vol. 55, pp. 169-179, 3// 2016.
- [3] P. Zhang and D. Lu, "A survey of condition monitoring and fault diagnosis toward integrated O&M for wind turbines," *Energies*, vol. 12, No. 14, p. 2801, 2019.
- [4] E. Artigao, A. Honrubia-Escribano, and E. Gómez-Lázaro, "In-Service Wind Turbine DFIG Diagnosis using Current Signature Analysis," *IEEE Transactions on Industrial Electronics*, Vol. 67, No. 3, pp. 2262-2271, 2020.
- [5] J. Maldonado-Correa, S. Martín-Martínez, E. Artigao, and E. Gómez-Lázaro, "Using SCADA Data for Wind Turbine Condition Monitoring: A Systematic Literature Review," *Energies*, Vol. 13, No. 12, p. 3132, 2020.
- [6] M.L. Hossain, A. Abu-Siada, and S. Muyeen, "Methods for advanced wind turbine condition monitoring and early diagnosis: A literature review," *Energies*, Vol. 11, No. 5, p. 1309, 2018.
- [7] W. Qiao and D. Lu, "A Survey on Wind Turbine Condition Monitoring and Fault Diagnosis-Part I: Components and Sub-systems," *IEEE Transactions on Industrial Electronics*, Vol. 62, No. 10, pp. 6536-6545, 2015.
- [8] Y. Chen et al., "Numerical Modeling, Electrical Characteristics Analysis and Experimental Validation of Severe Inter-Turn Short Circuit Fault Conditions on Stator Winding in DFIG of Wind Turbines," *IEEE Access*, Vol. 9, pp. 13149-13158, 2021.
- [9] Y. Jangho, L. Kwanghwan, L. Kwang-Woon, L. Sang Bin, and Y. Ji-Yoon, "Detection and Classification of Stator Turn Faults and High-Resistance Electrical Connections for Induction Machines," *Industry Applications, IEEE Transactions on*, Vol. 45, No. 2, pp. 666-675, 2009.
- [10] Y. Gritli, L. Zarri, C. Rossi, F. Filippetti, G. Capolino, and D. Casadei, "Advanced Diagnosis of Electrical Faults in Wound-Rotor Induction Machines," *IEEE Trans. Ind. Electron.*, Vol. 60, No. 9, pp. 4012-4024, 2013.
- [11] S.M.A. Cruz and A.J.M. Cardoso, "Multiple Reference Frames Theory: A New Method for the Diagnosis of Stator Faults in Three-Phase Induction Motors," *Energy Conversion, IEEE Transactions on*, Vol. 20, No. 3, pp. 611-619, 2005.
- [12] H. Douglas, P. Pillay, and P. Barendse, "The detection of interturn stator faults in doubly-fed induction generators," in *Conf. Rec. IEEE IAS Annu. Meeting*, 2005, Vol. 2, pp. 1097-1102.

- [13] D. Shah, S. Nandi, and P. Neti, "Stator-Interturn-Fault Detection of Doubly Fed Induction Generators using Rotor-Current and Search-Coil-Voltage Signature Analysis," *IEEE Trans. Ind. Appl.*, Vol. 45, No. 5, pp. 1831-1842, 2009.
- [14] L. Jun-qing, M. Li, and W. De-yan, "Influence of stator turn-to-turn short-circuit on magnetic field of DFIG," in *2011 International Conference on Electrical Machines and Systems*, 2011, pp. 1-5.
- [15] M. Yousefi Kia, M. Khedri, H.R. Najafi, and M.A.S. Nejad, "Hybrid modelling of doubly fed induction generators with inter-turn stator fault and its detection method using wavelet analysis," *IET Generation, Transmission and Distribution*, Vol. 7, No. 9, pp. 982-990, 2013.
- [16] G. Stojcic, K. Pasanbegovic, and T.M. Wolbank, "Detecting Faults in Doubly Fed Induction Generator by Rotor Side Transient Current Measurement," *IEEE Trans. Ind. Appl.*, Vol. 50, No. 5, pp. 3494-3502, 2014.
- [17] S. He, X. Shen, and Z. Jiang, "Detection and Location of Stator Winding Interturn Fault at Different Slots of DFIG," *IEEE Access*, Vol. 7, pp. 89342-89353, 2019.
- [18] S.J. Watson, B.J. Xiang, Y. Wenxian, P. J. Tavner, and C.J. Crabtree, "Condition Monitoring of the Power Output of Wind Turbine Generators using Wavelets," *IEEE Trans. Energy Convers.*, Vol. 25, No. 3, pp. 715-721, 2010.
- [19] S. Djurovic, C.J. Crabtree, P.J. Tavner, and A.C. Smith, "Condition monitoring of wind turbine induction generators with rotor electrical asymmetry," *IET J. Renew. Power Gen.*, Vol. 6, No. 4, pp. 207-216, 2012.
- [20] M.N. Zaggout, P.J. Tavner, C.J. Crabtree, and L. Ran, "Detection of rotor electrical asymmetry in wind turbine doubly-fed induction generators," *IET J. Renew. Power Gen.*, Vol. 8, No. 8, pp. 878-886, 2014.
- [21] Y. Gritli, C. Rossi, D. Casadei, F. Filippetti, and G.A. Capolino, "A Diagnostic Space Vector-based Index for Rotor Electrical Fault Detection in Wound-Rotor Induction Machines under Speed Transient," *IEEE Transactions on Industrial Electronics*, Vol. 64, No. 5, pp. 3892-3902, 2017.
- [22] R.K. Ibrahim, S.J. Watson, S. Djurović, and C.J. Crabtree, "An Effective Approach for Rotor Electrical Asymmetry Detection in Wind Turbine DFIGs," *IEEE Transactions on Industrial Electronics*, Vol. 65, No. 11, pp. 8872-8881, 2018.
- [23] A. Stefani, A. Yazidi, C. Rossi, F. Filippetti, D. Casadei, and G.A. Capolino, "Doubly Fed Induction Machines Diagnosis based on Signature Analysis of Rotor Modulating Signals," *IEEE Trans. Ind. Appl.*, Vol. 44, No. 6, pp. 1711-1721, 2008.
- [24] R. Roshanfekar and A. Jalilian, "Wavelet-based index to discriminate between minor inter-turn short-circuit and resistive asymmetrical faults in stator windings of doubly fed induction generators: a simulation study," (in En), *IET Generation, Transmission and Distribution*, Vol. 10, No. 2, pp. 374-381, 2015.
- [25] J. Faiz, S.M.M. Moosavi, M.B. Abadi, and S.M.A. Cruz, "Magnetic equivalent circuit modelling of doubly-fed induction generator with assessment of rotor inter-turn short-circuit fault indices," *IET Renewable Power Generation*, Vol. 10, No. 9, pp. 1431-1440, 2016.
- [26] S. M. Moosavi, J. Faiz, M.B. Abadi, and S.M.A. Cruz, "Comparison of rotor electrical fault indices owing to inter-turn short circuit and unbalanced resistance in doubly-fed induction generator," *IET Electric Power Applications*, Vol. 13, No. 2, pp. 235-242, 2019.
- [27] G. Abad, J. Lopez, M. Rodriguez, L. Marroyo, and G. Iwanski, *Doubly Fed Induction Machine: Modeling and Control for Wind Energy Generation*. Hoboken, New Jersey: Wiley, 2011.
- [28] A. Bellini, F. Filippetti, C. Tassoni, and G.A. Capolino, "Advances in Diagnostic Techniques for Induction Machines," *IEEE Trans. Ind. Electron.*, Vol. 55, No. 12, pp. 4109-4126, 2008.